Published in final edited form as:
Anal Chem. 2008 December 15; 80(24): 9830–9834. doi:10.1021/ac8021899.

Confocal, 3-Dimensional Tracking of Individual Quantum Dots in High Background Environments

Nathan P. Wells, **Guillaume A. Lessard**, and **James H. Werner***
Center for Integrated Nanotechnologies (MPA-CINT), Los Alamos National Laboratory, Los Alamos, New Mexico 87545, USA

Abstract

We demonstrate a custom confocal fluorescence-microscope that is capable of tracking individual quantum dots undergoing three dimensional Brownian motion (diffusion coefficient ~0.5 $\mu m^2/s$) in environments with a signal-to-background ratio as low as 2:1, significantly worse than observed in a typical cellular environment. By utilizing a pulsed excitation source and time-correlated single photon counting, the time-resolved photon stream can be used to determine changes in the emission lifetime as a function of position and positively identify single quantum dots via photon-pair correlations. These results indicate that this microscope will be capable of following protein and RNA transport throughout the full 3 dimensional volume of a live cell for durations up to 15 seconds.

Introduction

Single-molecule detection, particularly via laser induced fluorescence, has matured over the last two decades to a point that *in vivo* assays are routinely accessible.1–4 Of particular interest to biologists and biophysicists are *in vivo* observations of proteins, RNA, DNA, and viruses performing biological functions.3, 5–7 To this extent, observing single-molecule fluorescence via camera based wide field microscopy has been used to study biological events in two-dimensions (2D), particularly membrane dynamics,4, 5, 8–10 and in at least one instance has been extended to three-dimensions (3D) with limited (≤1 μm) depth of field.11 While camera based techniques can have very good 2D localization accuracy (< 50 nm) and have proven effective when studying molecules limited to motions in the focal plane, many biologically important functions involve molecular transport that is inherently 3D in nature.

A handful of research groups have recently described closed-loop 3D tracking microscopes with particle position feedback based on a combination of off-focus imaging, confocal detection, and fluorescence modulation/demodulation.11–16 Pioneering work in this field was geared towards tracking individual bacteria,17 with more recent studies and instruments being developed for tracking nanoparticles of colloidal gold,13 fluorescent beads12, 14 or individual quantum dots.14–16 In particular, Mabuchi and co-workers have recently demonstrated tracking of individual quantum dots with simultaneous collection of photon-

*electronic address: jwerner@lanl.gov

statistics to show, for the first time, antibunching from a single quantum dot freely moving in solution.16 The modulation/demodulation approach taken by Mabuchi and co-workers utilizes a large excitation beam waist (1.5–3 μm) and non-confocal detection which will suffer in environments with high background levels, such as those encountered in certain cell types and cell lines. In contrast, we have previously reported on a 3D tracking microscope based on confocal detection that could track single quantum dots diffusing near 1 $\mu m^2/s$.15 Our confocal approach has a number of advantages for *in vivo* tracking studies, including smaller excitation volumes and lower incident excitation powers, which help reduce the auto-fluorescent background and reduce photo-toxic effects for future live cell microscopy.

Existing 3D tracking methods have not yet, to our knowledge, experimentally explored the effects of a homogeneous background signal. In 2D camera based tracking, the presences of a fluorescent background degrades the localization accuracy in each image.18 For the existing 3D fluorescence modulation/demodulation techniques,12, 16 tracking in a high background may be possible; however, since this technique sweeps the laser in a circle, the effective probe volume is much larger than the single confocal volume we employ here. Given the same concentration of background fluorescent emitters, techniques that sweep the laser will cause the single-particle signal to background level be much worse than our single confocal volume.

In this paper we demonstrate the ability to track single quantum dots in a high background environment. Specifically, we are able to track individual CdSe/ZnS core-shell dots in mixtures of glycerol:water and glycerol:fetal-bovine-serum (FBS). The glycerol:FBS mixture has an auto-fluorescence background 25 times larger than that of glycerol:water, which reduces the average signal-to-background ratio of quantum dot fluorescence from 50:1 to 2:1. In both cases we observe trajectories of up to 15 s in duration. By simultaneously recording time-resolved emission statistics, we can confirm that the emission comes from individual dots via photon-pair correlation measurements19, 20 and can measure emission dynamics of individual dots as a function of position with approximately 100 ps time-resolution.

Experimental

Quantum Dot Samples

Water soluble quantum dots (Qdot 605 ITK amino (PEG)) were purchased from Invitrogen. The average diameter of the core-shell CdSe/ZnS dots was 16.5 ± 1.8 nm, measured with fluorescence-correlation spectroscopy (FCS) calibrated with 41 nm diameter fluorescent microspheres (PolySciences YG microspheres). The quantum dot brightness-per-particle in the tracking microscope saturated at 64 kHz with 15–20 μW incident pump power. Solutions of glycerol:water and glycerol:FBS were made close to 80% glycerol by weight. The viscosity of the solutions, measured with a falling ball viscometer at 295 K, were 45 and 57 cP respectively. The concentration of quantum dots in the solutions used for tracking was 20 pM, which allowed the tracking apparatus to start 2–3 tracks per minute.

Particle Position and Feedback

The confocal tracking microscope has been described previously.15, 21 The experiment is built on an inverted microscope platform (Olympus IX-71). A 470 nm pulsed diode laser (PicoQuant LDH-P-C-470B) running at 10 MHz and 15–20 μW average power is directed into the microscope platform with a dichroic beam splitter (Chroma 505DXCT) and focused by a water-immersion objective (NA=1.2, M=60) to a beam waist (w_0) of 500 nm in the sample. The light collected and transmitted though the dichroic beam splitter is filtered through an emission bandpass filter (Chroma HQ620/60 X) prior to being focused with an externally mounted tube lens (22.5 cm focal length singlet). Determining and encoding of the particle's 3D position is based upon detecting its emitted fluorescence through four spatially arranged pinholes (Figure 1). The emission is split and imaged onto two identical fiber-bundles. These fiber-bundles consist of two 50 μm diameter optical fibers with a center-to-center fiber separation of ≈ 55 μm that act as spatial filters for a single element detector associated with each fiber. Of particular importance is that one pair of spatial filters is at a slightly different distance to the tube lens than the other pair, enabling positional sensitivity in Z. The four optical fibers are coupled to single-photon-counting avalanche photodiodes (PerkinElmer SPCM-AQR-14), which are read by pulse counting electronics (National Instruments PCI-6602, Becker & Hickl SPC630). For each time step in a trajectory, the counts on each detector are integrated for 5 ms, processed through an algorithm implemented in LabVIEW Real-Time, and the XYZ positioning stage (Physik Instrumente P-733.3DD) is moved to reposition the emitter toward the laser focus. The per-photon time-tagged, time-resolved information from the SPC630 is used to post-process lifetime and photon pair correlation data for each trajectory.20

The tracking algorithm's feedback is based on Proportional-Integral-Differential (PID) principles. We denote the four fiber-pinholes and associated detectors D_0−D_3. The fiber-bundle detecting the transmitted emission leads to detectors D_0 and D_1, while the fiber-bundle detecting the reflected emission leads to detectors D_2 and D_3. Positional sensitivity along the X and Y axes is achieved by detecting a difference in the number of photons observed through a single fiber-bundle ($D_0 - D_1$ for X or $D_2 - D_3$ for Y). The two fiber-bundles are oriented orthogonally with respect to one another to enable a differential signal for the X and Y Cartesian coordinate axes. The path lengths between the beam splitter and the two fiber-bundles is unequal, allowing the observation of two focal planes in sample space that are separated by ≈ 200 nm. This feature allows positional sensitivity in Z by detecting a difference in the number of photons observed between the two z slices ($[D_0+D_1]-[D_2+D_3]$).

The tracking algorithm calculates the error signal for each axis (E_X, E_Y, E_Z) according to Equation 1. For 3D Brownian diffusion we only use the proportional (P) term of PID feedback. The controller gain in the PID feedback (K_i; $i = \{X, Y, Z\}$) for each axis is determined from tracking simulations including the experimentally determined three dimensional collection efficiency function (CEF).22 The collection efficiency function is a map of the relative number of photons collected from an emitter at all points in the probe volume. We experimentally determine the CEF by scanning an immobilized (in polydimethysiloxane) quantum dot with the XYZ stage. The scan range for the for the

experimental data in Figure 2 was 3 μm (100 nm steps) in X and Y and 4 μm (200 nm steps) in Z. Each pixel was integrated for 30 ms and photon counts on each detector were recorded separately. In our previous reports, a theoretical calculation of the CEF was used to determine the appropriate gain parameters.21 Here, the experimentally measured 3D CEF for each detector is used to find these values. This change has enabled longer and more robust three dimensional tracking over our previous experimental report.15 A representation of the error signals (Equation 1) for each axis are shown in Figure 2. The error signals are calculated from line-slices down the CEF while holding the other two axes at zero. The step size for each axis in the PID algorithm is calculated by multiplying the error signals (Equation 1) by the controller gain. The the controller gain values (K_i's) used here are K_X=0.35, K_Y=0.35, K_Z=0.75 microns, determined from Monte Carlo simulations21 using the experimentally measured 3D CEF.

$$\begin{aligned} E_X &= \frac{D_0 - D_1}{D_0 + D_1} \\ E_Y &= \frac{D_2 - D_3}{D_2 + D_3} \\ E_Z &= \frac{(D_0 + D_1) - (D_2 + D_3)}{D_0 + D_1 + D_2 + D_3} \end{aligned} \quad (1)$$

Results and Discussion

Example trajectories in glycerol:water and glycerol:FBS are shown in Figure 3 and Figure 4 respectively. The average background count rate summed on all four detectors for glycerol: water was 800 Hz, largely coming from detector dark counts, while for glycerol:FBS the average background count rate was 20 kHz stemming from fluorescence of the FBS. Using simulations developed previously,21 we estimate the average tracking error to be 70 nm in X and Y and 110 nm in Z for both of the experimentally observed background count rates. The insensitivity of tracking error to the S/N stems from the fact that the background is a homogeneous noise source that adds a constant level to each detector. By utilizing a differential feedback system (Equation 1) to estimate the particle's position, the background is largely subtracted out and the tracking error is dominated by the shot noise of the quantum dot emission rate.

Particle trajectories can be classified as pure Brownian diffusion or directed motion through an analysis of their mean-squared displacement (MSD) over time.8 The *MSD* is given by $MSD(\Delta t) = \langle [S(t+\Delta t) - S(t)]^2 \rangle$, where $S(t) = (x(t), y(t), z(t))$ represents the particle's three-dimensional coordinates as a function of time. *MSD* data calculated from the trajectories are shown in Figure 3c and Figure 4c. For three dimensional diffusive motion, the *MSD* is linear in Δt with a slope of 6D. A linear fit of the *MSD* for the first quarter of the trajectory displacements is used to determine the diffusion coeffiscient, D. We choose to only use the first quarter of the *MSD* data since at longer times the *MSD* suffers from substantial noise, due to the fact that fewer points can be used to calculate the *MSD* as the total duration is approached. This is a standard practice in the single particle tracking field.8 Linear fits of the two data sets give a diffusion coefficient of 0.47 $\mu m^2/s$ in glycerol:water (45 cP) and 0.37 $\mu m^2/s$ in glycerol:FBS (57 cP). The experimental values are consistent with the Stokes-Einstein relationship, which predicts average diffusion coefficients of 0.58 and 0.46 $\mu m^2/s$ for the two solutions respectively. We discuss the distribution of diffusion coefficients

obtained using two different methods, the MSD8 and a maximum likelihood analysis,23 further below and in the Supporting Information.

Trajectories of individual quantum dots may be identified via photon-pair correlation, where the histogram of time delays between successive photons is measured.19, 20 The photon-pair correlations are shown in Figure 3d and Figure 4d. A suppression in measuring successive photons arriving with a time delay less than the lifetime (antibunching) is used to quantify the number of independent emitters (N_e). The number of independent emitters is given by $N_e = \left[1 - \frac{A_c}{A_s}\right]^{-1}$, where A_c and $\bar{A}_s$ are respectively the center-peak area and the average satellite-peak area.20

In the case of glycerol:water (Figure 3) N_e = 1.17, clearly showing that the tracked fluorescent particle is a single quantum dot. In contrast, tracking data in glycerol:FBS (Figure 4) initially indicate that N_e = 2.22. However, in the presence of a large background, antibunching will be suppressed as photons may arrive in pairs near zero time delay due to detecting two background photons or one background photon and one fluorescence photon from the molecule under investigation. We used equation 4 of Weston *et al*.20 to correct N_e for the large background count rate encountered in the FBS mixture; using this method the corrected number of independent emitters for the data of Figure 4 is 0.99. In addition, comparing Figure 3d and Figure 4d shows that measurements taken with a large auto-fluorescence background have narrower peaks in the photon pair correlation histogram, reflecting the shorter lifetime of auto-fluorescence compared to quantum dot fluorescence. The narrowness of the central-peak compared to the satellite-peaks, given similar heights, in Figure 4d further supports that its origin is mostly background fluorescence and that the trajectory is from a single quantum dot.

In both Figure 3 and Figure 4 the observed count rate on the four detectors rapidly fluctuates between the expected single particle brightness level and the background level. To demonstrate that the fluctuations in the count rate are largely due to changes in the dot's photophysics, in this case blinking,24–30 rather than the tracking algorithm losing and reacquiring the quantum dot, we can use the time resolved photon data to look for changes in the quantum dot's lifetime. Prior studies have shown that blinking dynamics (dark periods) are driven by a dynamic increase in the non-radiative relaxation rate causing a drop in the emission lifetime.25, 28, 30 We investigate whether dynamic changes in emission lifetime can be observed in these 3D trajectories by estimating the quantum dot's fluorescence lifetime using a single exponential Maximum Likelihood Estimator (MLE)31 for photons binned in 25 ms intervals (Figure 5). Figure 5 demonstrates that the quantum dot lifetime is fluctuating during the trajectory. The lifetime fluctuates around a mean value of 10 ns with some large dynamic decreases that are significantly correlated to the observed count rate. This is a strong indication that the count rate fluctuations are caused by quantum dot blinking and not tracking error (Movie M1.mov, Supporting Information).

The data from the two selected trajectories demonstrates that the tracking microscope is capable of tracking individual quantum dots even in the presence of a high auto-fluorescence background. To give a broader representation of the data, we show the distribution of

measured diffusion coefficients for trajectories in glycerol:FBS (Figure 6). Since the MSD analysis demonstrates the motion is purely diffusive (Fig. 3c,Fig 4c), one can use a maximum likelihood analysis,23 in addition to MSD analysis,8 to determine the diffusion coefficient for each trajectory. The average value of D for the trajectories is 0.37 $\mu m^2/s$ for both the *MSD* and MLE analysis. Both the *MSD* and MLE methods give a mean value consistent with our independent measurements of the average quantum dot diameter and solution viscosity. The width of the distribution does depend on the chosen method. The MLE generally gives a narrower distribution than MSD,23 however, the *MSD* width is consistent with simulations of a single sized particle undergoing a 3D random walk (Figure S-5, Supporting Information) when using the same (*MSD*) analysis method. We provide diffusion coefficient distributions along each axis using both MSD and MLE in Figure S-7 (Supporting Information). Both methods are consistent and show that diffusion along each axis is unbiased; there is no systematic error causing the microscope to prefer to track in one axis over another.

The distribution of trajectory durations in glycerol:FBS is given in Figure 6 (RHS). The normalized cumulative integral of the trajectory duration distribution shows that half the trajectories have a duration greater than 2.2 s and that the probability of observing a trajectory lasting greater than 10 s is substantial (16%). The distribution of trajectory durations essentially follows an exponential distribution with a decay time τ =2.05 s. An exponential decay in track durations can be readily explained as having a certain probability of losing the quantum dot during any given 5 ms integration period. If the probability to lose a dot during this integration period is P_{lost}, then the probability to have a duration "N" 5 ms intervals long is simply:

$$\begin{array}{ll} P(N) & =(1-P_{lost})^N=\exp(-N\tau^{-1}) \\ \tau^{-1} & =\ln(\frac{1}{1-P_{lost}}). \end{array} \quad (2)$$

As can be seen, the duration of measured trajectories is expected to decay exponentially. From the exponential fit to the trajectory duration data, we obtain a value for losing the dot during any 5 ms single step in the tracking experiments, P_{lost} of 2.4×10^{-3}. We note that this value is very close to the probability that a quantum dot enters a dark period for a duration of 5 ms or greater.27 Given the above, we have concluded our ability to track individual quantum dots is limited primarily by photophysical blinking for time periods greater than our integration time and not mistakes in estimating the quantum dot's current position in the optical probe volume (See Supporting Information, Movie M1). Future research directions could use additives such as propyl galate30 to try to further suppress blinking or could use new quantum dots that have thicker shells32 that are less prone to having an electron or hole tunnel to a surface defect site, which should enable 3D trajectories of greater duration.

Conclusions

We have shown that single-molecule tracking is possible in high background environments using a confocal 3D tracking microscope. In the current demonstration, trajectories recorded in high background samples had essentially the same tracking error as those with little to no

background. The independence of tracking error reported here with respect to S/N is one key advantage of using single point detectors with differential feed-back control. The signal to background ratio in this demonstration is significantly higher than those typically encountered in live cells and suggests that tracking single quantum dots in live cells will not be limited by the presence of cellular auto-fluorescence.

In addition we have demonstrated the ability to measure dynamic fluctuation in the lifetime of a single quantum dot due to blinking. More generally, one could use the same information to detect fluctuations in protein structure,33 changes in cellular environment using non-blinking fluorophores,32 or intracellular detection of protein-protein or protein-RNA interactions with three dimensional spatial resolution. While we feel the primary applications of this microscope lie in monitoring protein traffic, interactions, and conformations inside living cells, we also note that this instrument could be used to monitor individual protein conformation (for long time periods) without resorting to sample immobilization as has already been demonstrated with ex-vivo particle and molecule feedback systems.34, 35

Supplementary Material

Refer to Web version on PubMed Central for supplementary material.

Acknowledgement

This work is supported by the National Institutes of Health (No. R21AI07707) and the National Nanotechnology Enterprise Development Center (NNEDC). This work was performed at the Center for Integrated Nanotechnologies, a U.S. Department of Energy, Office of Basic Energy Sciences user facility. Los Alamos National Laboratory is operated by Los Alamos National Security, LLC, for the National Nuclear Security Administration of the U.S. Department of Energy under contract DE- AC52-06NA25396. We thank Peter Goodwin for advice and a critical reading of this manuscript.

References

1. Moerner WE, Fromm DP. Rev. Sci. Instrum. 2003; 74:3597–3619.
2. Goodwin PM, Ambrose WP, Keller RA. Acc. Chem. Res. 1996; 29:607–613.
3. Michalet X, Pinaud FF, Bentolila LA, Tsay JM, Doose S, Li JJ, Sundaresan G, Wu AM, Gambhir SS, Weiss S. Science. 2005; 307:538–544. [PubMed: 15681376]
4. Dahan M, Levi S, Luccardini C, Rostaing P, Riveau B, Triller A. Science. 2003; 302:442–445. [PubMed: 14564008]
5. Fujiwara T, Ritchie K, Murakoshi H, Jacobson K, Kusumi A. J. Cell Biol. 2002; 157:1071–1081. [PubMed: 12058021]
6. Femino AM, Fay FS, Fogarty K, Singer RH. Science. 1998; 280:585–590. [PubMed: 9554849]
7. Seisenberger G, Ried MU, Endress T, Buning H, Hallek M, Brauchle C. Science. 2001; 294:1929–1932. [PubMed: 11729319]
8. Saxton MJ, Jacobson K. Annu. Rev. Biophys. Biomol. Struct. 1997; 26:373–399. [PubMed: 9241424]
9. Lidke DS, Andrews NL, Pfeiffera JR, Jones HDT, Sinclair MB, Haaland DM, Burns AR, Wilson BS, Oliver JM, Lidke KA. Proc. SPIE. 2007; 6448 64480Y1-64480Y1-8.
10. Cheezum MK, Walker WF, Guilford WH. Biophys. J. 2001; 81:2378–2388. [PubMed: 11566807]
11. Holtzer L, Meckel T, Schmidt T. Appl. Phys. Lett. 2007; 90:053902-1–053902-3.
12. Levi V, Ruan Q, Gratton E. Biophys. J. 2005; 88:2919–2928. [PubMed: 15653748]
13. Cang H, Wong CM, Xu CS, Rizvi AH, Yang H. Appl. Phys. Lett. 2006; 88:223901-1–223901-3.

14. Cang H, Xu CS, Montiel D, Yang H. Opt. Lett. 2007; 32:2729–2731. [PubMed: 17873950]
15. Lessard GA, Goodwin PM, Werner JH. Appl. Phys. Lett. 2007; 91:224106-1–224106-3.
16. McHale K, Berglund AJ, Mabuchi H. Nano Lett. 2007; 7:3535–3539. [PubMed: 17949048]
17. Berg HC. Rev. Sci. Instrum. 1971; 42:868–871. [PubMed: 4940742]
18. Thompson RE, Larson DR, Webb WW. Biophys. J. 2002; 82:2775–2783. [PubMed: 11964263]
19. Kimble HJ, Dagenais M, Mandel L. Phys. Rev. Lett. 1977; 39:691–695.
20. Weston K, Dyck M, Tinnefeld P, Muller C, Herten DP, Sauer M. Anal. Chem. 2002; 74:5342–5349. [PubMed: 12403591]
21. Lessard GA, Goodwin PM, Werner JH. Proc. SPIE. 2006; 6092:609205-1–609205-8.
22. Qian H, Elson EL. Appl. Opt. 1991; 30:1185–1195. [PubMed: 20582127]
23. Montiel D, Cang H, Yang H. J. Phys. Chem. B. 2006; 110:19763–19770. [PubMed: 17020359]
24. Nirmal M, Dabbousi BO, Bawendi MG, Macklin JJ, Trautman JK, Harris TD, Brus LE. Nature. 1996; 383:802–804.
25. Fisher BR, Eisler HJ, Stott NE, Bawendi MG. J. Phys. Chem. B. 2004; 108:143–148.
26. Kuno M, Fromm DP, Hamann HF, Gallagher A, Nesbitt DJ. J. Chem. Phys. 2001; 115:1028–1040.
27. Kuno M, Fromm DP, Hamann HF, Gallagher A, Nesbitt DJ. J. Chem. Phys. 2000; 112:3117–3120.
28. Zhang K, Chang H, Fu A, Alivisatos AP, Yang H. Nano Lett. 2006; 6:843–847. [PubMed: 16608295]
29. Cichos F, von Borczyskowski C, Orrit M. Curr. Opin. Colloid Interface Sci. 2007; 12:272–284.
30. Fomenko V, Nesbitt DJ. Nano Lett. 2008; 8:287–293. [PubMed: 18095736]
31. Tellinghuisen J, Wilkerson CW Jr. Anal. Chem. 1993; 65:1240–1246.
32. Chen Y, Vela J, Htoon H, Casson JL, Werder DJ, Bussian DA, Klimov VI, Hollingsworth JA. J. Am. Chem. Soc. 2008; 130:5026–5027. [PubMed: 18355011]
33. Werner JH, Joggerst R, Dyer RB, Goodwin PM. Proc. Nat. Acad. Sci. U.S.A. 2006; 103:11130–11135.
34. Cohen AE, Moerner WE. Opt. Express. 2008; 16:6941–6956. [PubMed: 18545398]
35. Cohen AE, Moerner WE. Proc. Nat. Acad. Sci. U.S.A. 2007; 104:12622–12627.

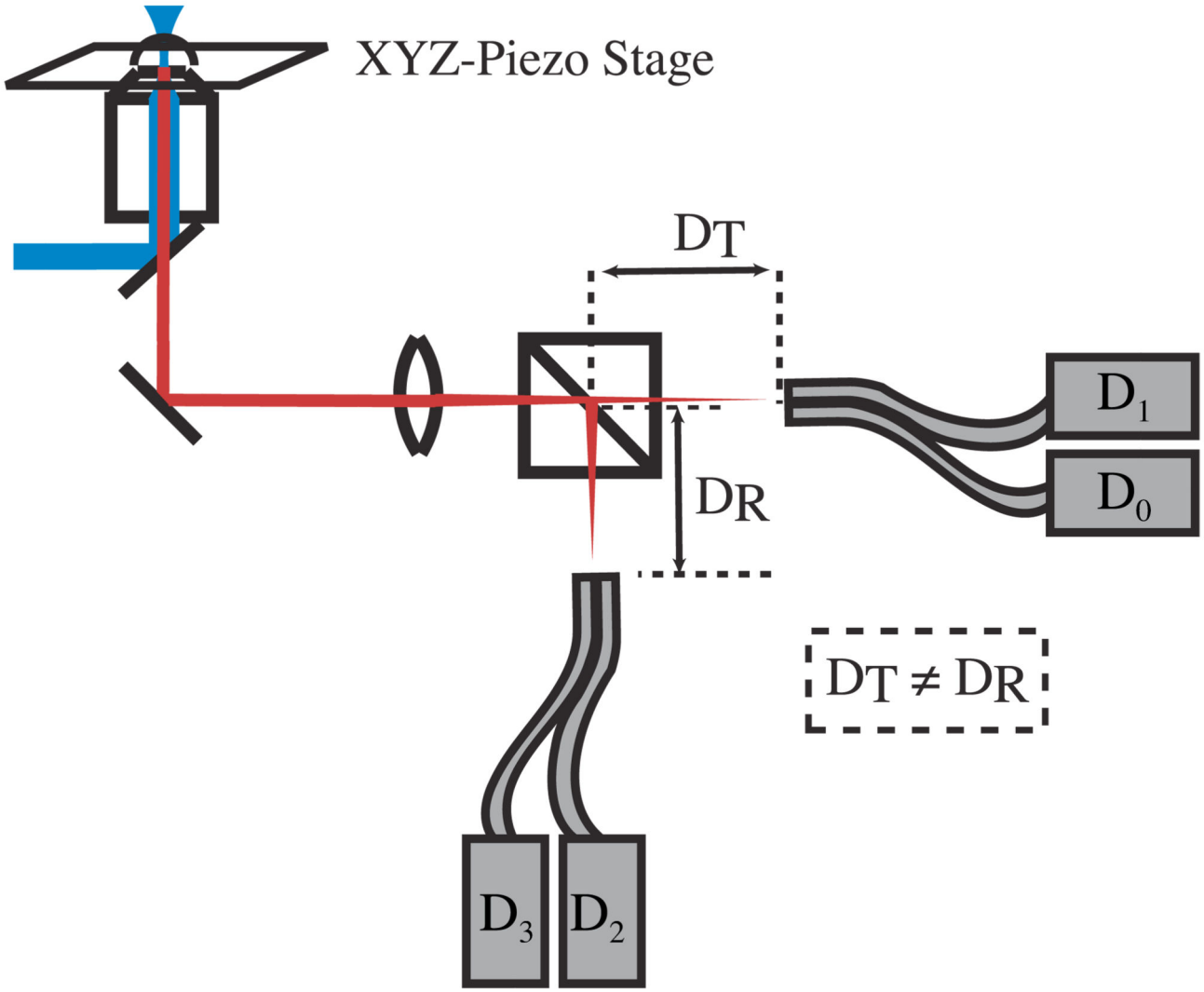

Figure 1.

3D-Tracking detection system and pinhole arrangement. Two fiber bundles described in the text are used as the four spatial pinholes for particle position detection. $D_0 - D_3$ are single-photon-counting avalanche photodiodes.

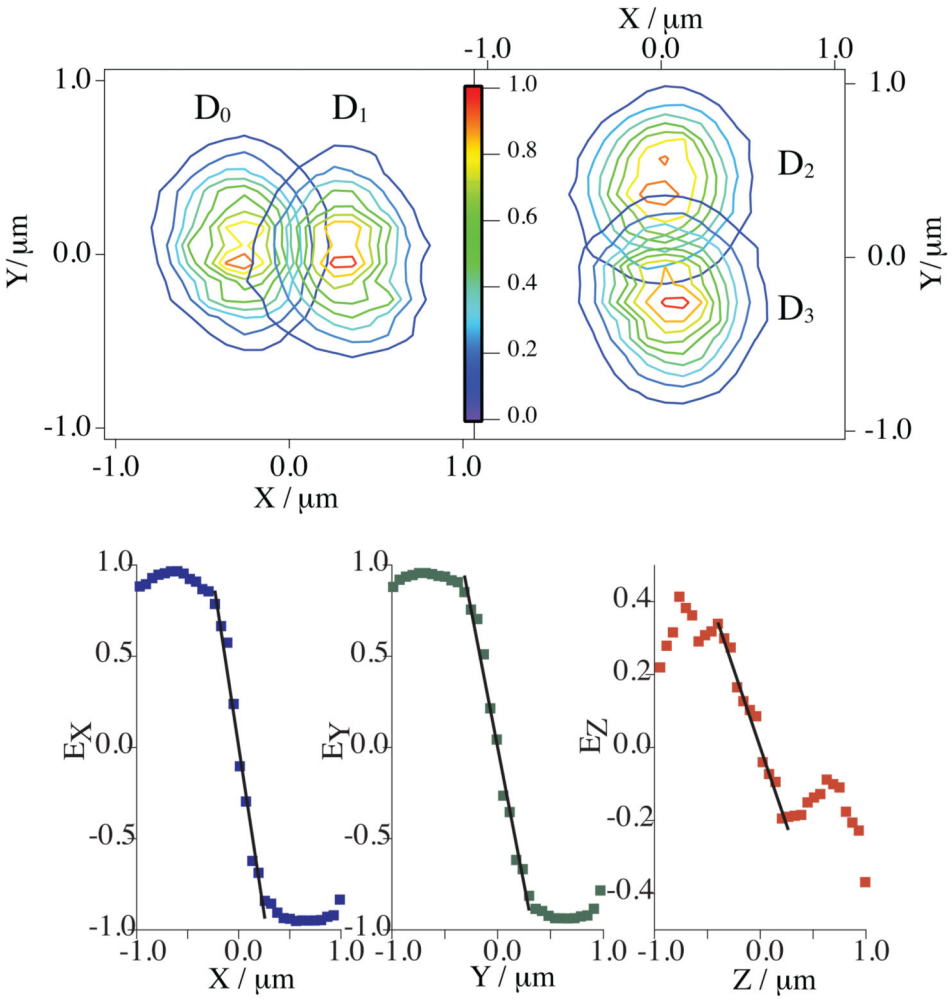

Figure 2.

Top: Tracking microscope collection efficiency function (CEF) near Z=0 measured through 4 fibers. Transmitted emission: fibers/detectors D_0 and D_1. Reflected emission: fibers/detectors D_2 and D_3. Data collected from a quantum dot immobilized in polydimethylsiloxane. Peak count rates are normalized to 1. For a single quantum dot at the origin, the count rate is ~ 64 kHz spread amongst all four detectors. Bottom: Error signals (Solid Squares) from Equation 1 for the three Cartesian axes calculated from line scans through the experimental CEF. Black solid lines are linear fits to the linear portion of the error signals. The linear slopes for X,Y and Z are −3.7,−3.0.−0.90 respectively. Error signals interpolated from the scanned CEF data.

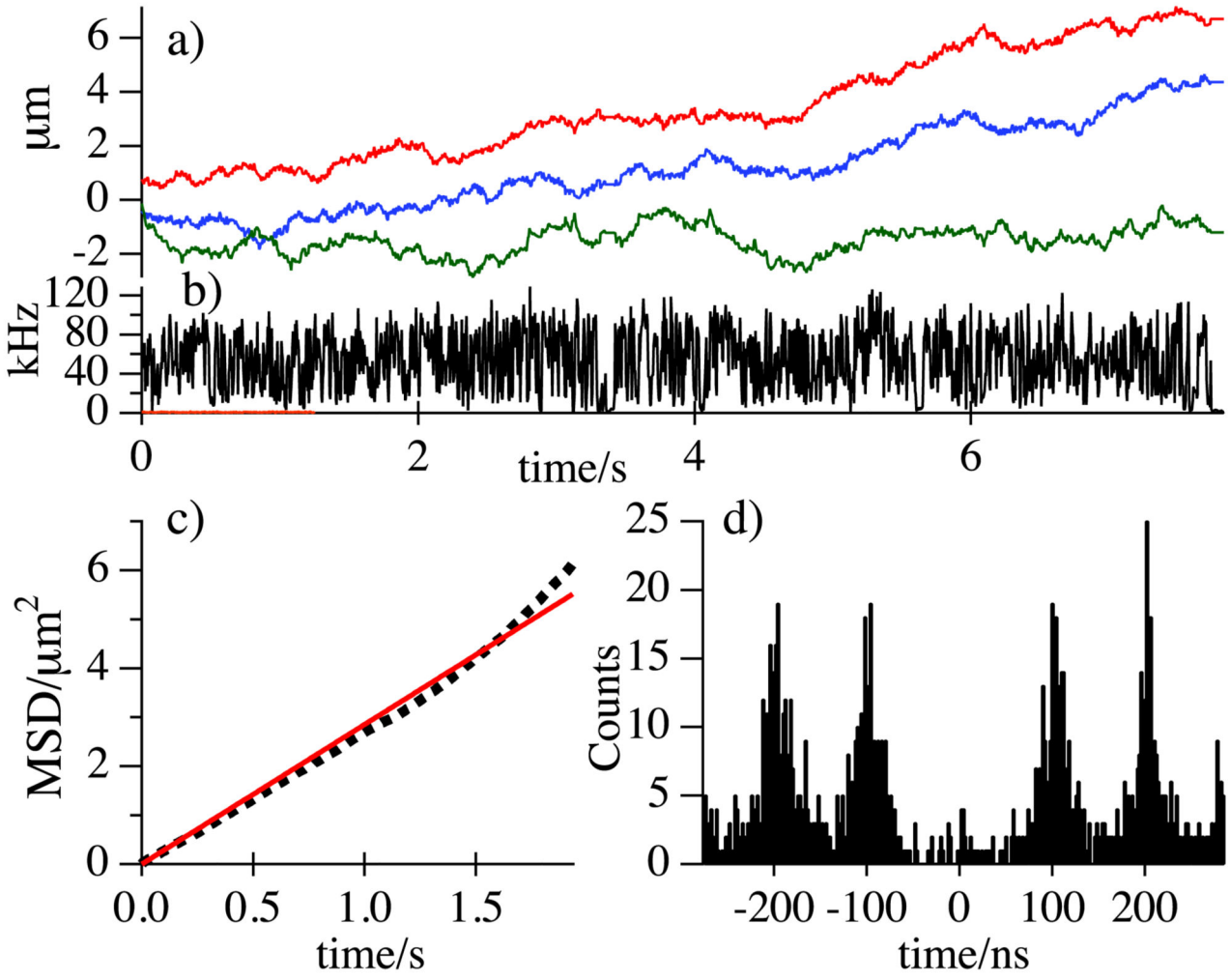

Figure 3.

Tracking Data in glycerol:water. a) Trajectory vs time. Stage Positions: *x(t)* (Red), *y(t)* (Blue), *z (t)* (Green). b) Count Rates. Black: Total Count Rate, Orange: Sample Background Count Rate. c) MSD vs time. Black: MSD, Red: Linear Fit. d) Photon-Pair Correlation, histogram of interphoton time delay. Suppression of events with near zero interphoton time delay shows antibunching behavior and demonstrates that the tracked particle is a single quantum dot.

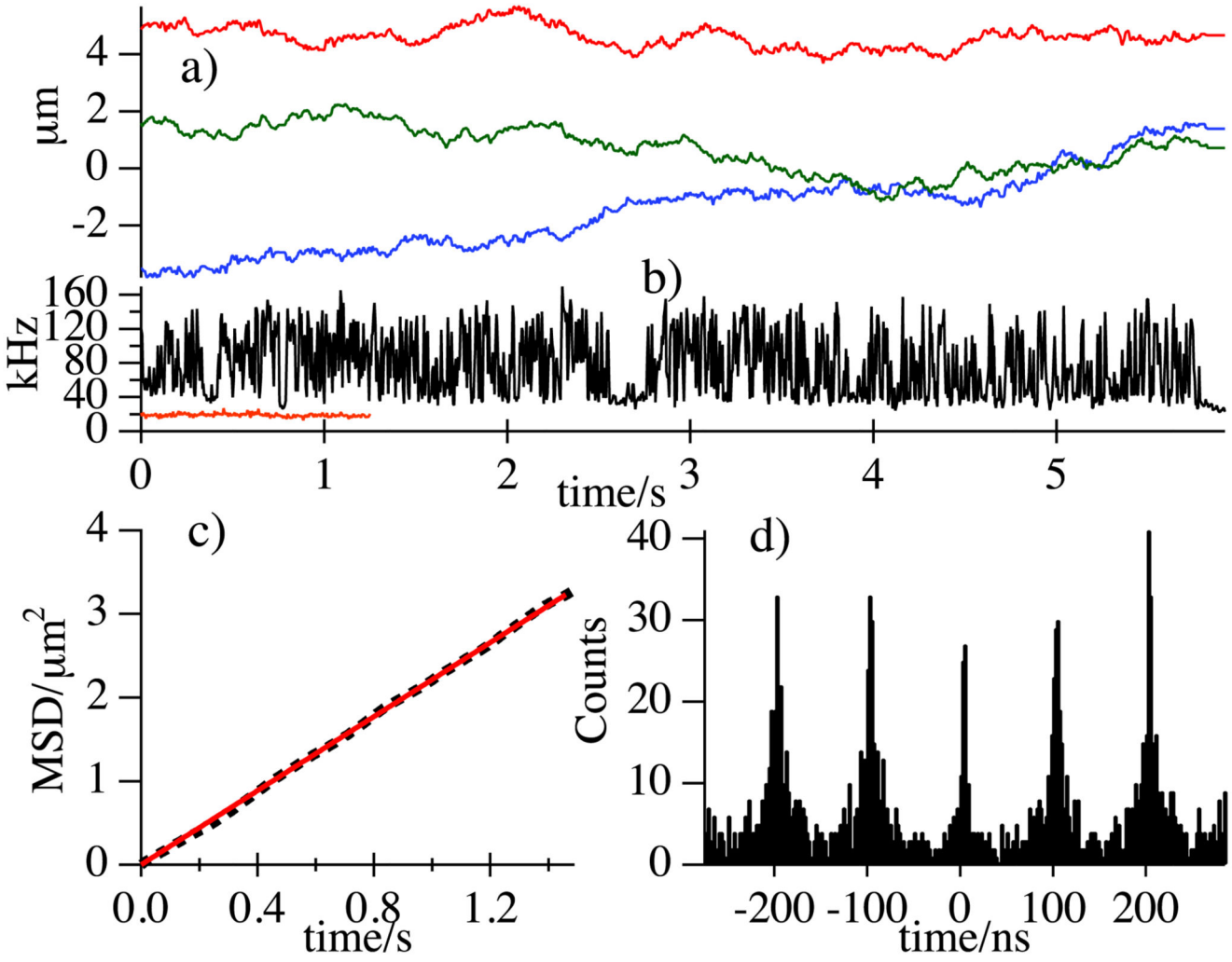

Figure 4.

Tracking Data in glycerol:FBS. a) Trajectory vs time. Stage Positions: *x(t)* (Red), *y(t)* (Blue), *z (t)* (Green). b) Count Rates. Black: Total Count Rate, Orange: Sample Background Count Rate. c) MSD vs time. Black: MSD, Red: Linear Fit. d) Photon-Pair Correlation, histogram of interphoton time delay. The background causes the central peak to grow, obscuring the expected behavior for a single quantum dot.

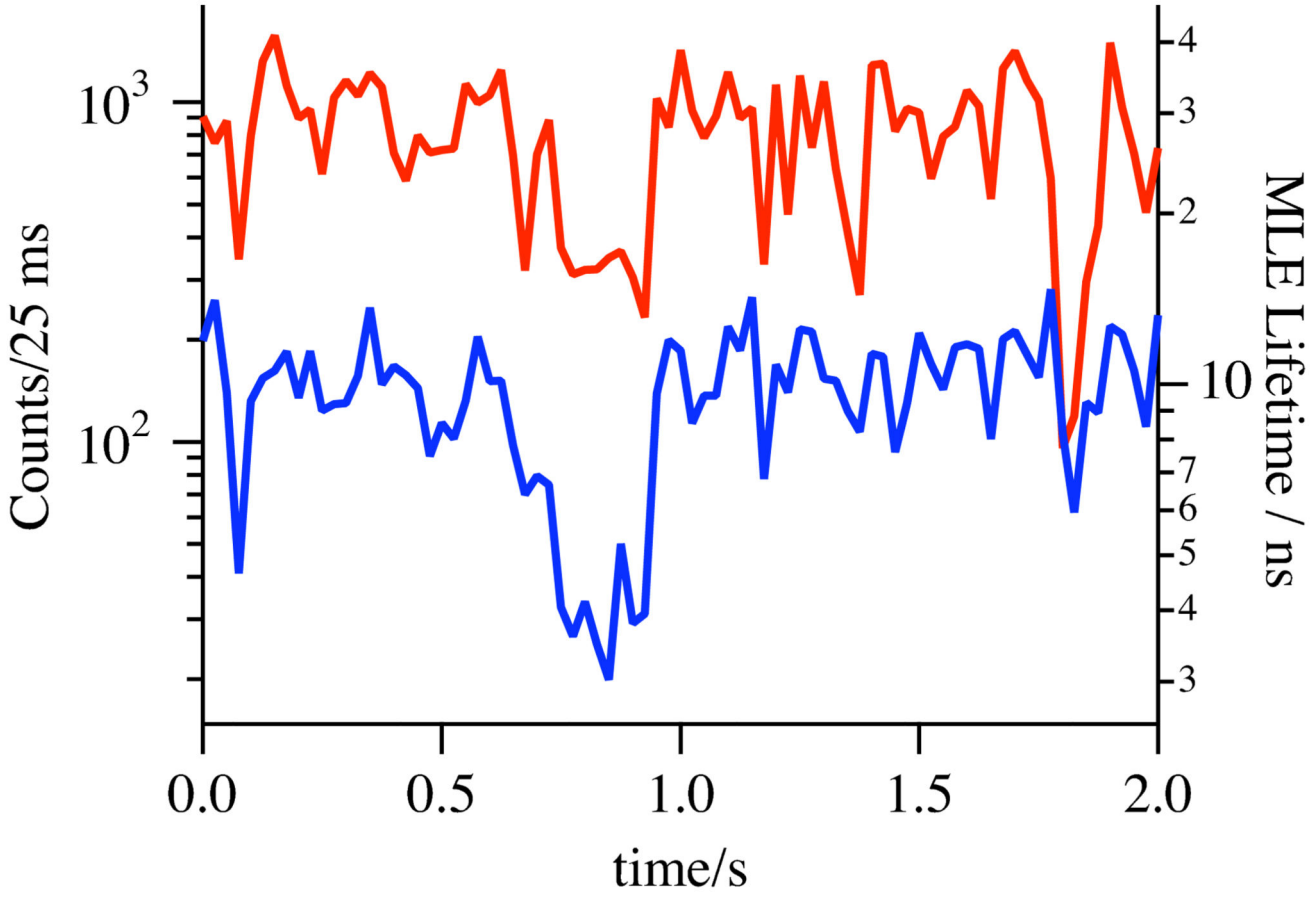

Figure 5.

Trajectory Count Rate (Red). Maximum Likelihood Estimator Lifetime (Blue). Data from a single-trajectory in glycerol:water binned per 25 ms. The two data sets have a Pearson's correlation coefficient of 0.65, showing significant correlation even at the 99% confidence interval.

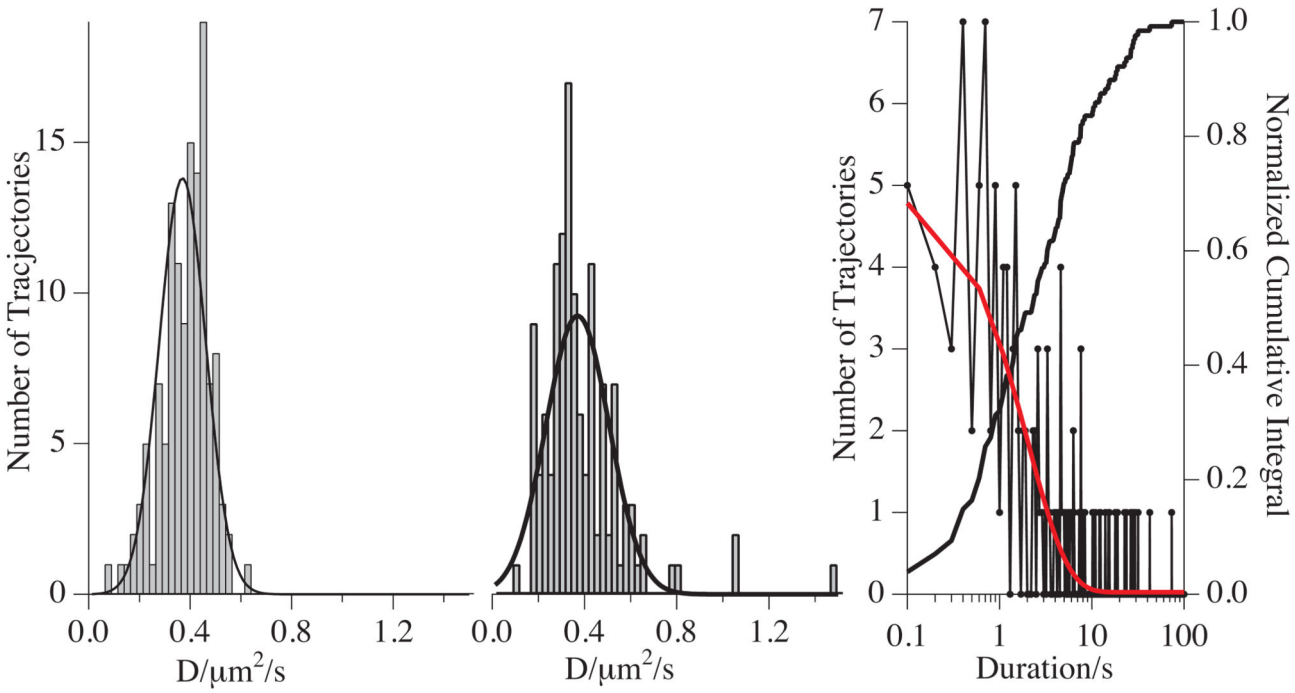

Figure 6.

Histogram of single trajectory diffusion coefficients (D) extracted from MLE analysis. Solid line: Gaussian fit of the MLE generated distribution centered at D=0.37 μm^2/s with a width of 0.13 μm^2/s. Middle: Histogram of single trajectory diffusion coefficients (D) extracted from MSD analysis. Solid line: Gaussian fit of the MSD generated distribution centered at D=0.37 μm^2/s with a width of 0.20 μm^2/s. Right: Histogram (line through points) of single trajectory durations. Red line is an exponential fit with τ=2.05 s. Thick black line is the cumulative integral of the histogram (normalized).